2009

# Phase transformations in (111) Si after spherical indentation

Ayesha J. Haq
*University of Wollongong*, ayesha@uow.edu.au

Paul G. Munroe
*The University of New South Wales*

# Phase transformations in (111) Si after spherical indentation

Ayesha J. Haq[a] and P.R. Munroe
*School of Materials Science and Engineering, University of New South Wales, Sydney, New South Wales 2052, Australia*

(Received 7 October 2008; accepted 6 January 2009)

Phase transformations in (111) Si after spherical indentation have been investigated by cross-sectional transmission electron microscopy. Even at an indentation load of 20 mN, a phase transformation zone including the high-pressure crystalline Si phases was observed within the residual imprints. The volume of the transformation zone, as well as that of the crystalline phases increased with the indentation load. Below the transformation zone, slip was found to occur on {311} planes rather than on {111} planes, usually observed on indentation of (100) Si. The distribution of defects was asymmetric, and for indentation loads up to 80 mN, their density was significantly lower than that reported for (100) Si. The experimental observations correlated well with modeling of the applied stress through ELASTICA.

## I. INTRODUCTION

It has been well established[1–7] that during loading, the diamond cubic silicon (Si-I) transforms to the metallic (Si-II) phase, accompanied by a volume reduction, which produces a displacement (or pop-in) in the loading curve. On unloading, depending on the indentation load and unloading rate, either amorphous silicon (a-Si) or a mixture of the high-pressure crystalline Si-III and Si-XII phases form, causing either an elbow or a pop-out, respectively, in the unloading curves. These metastable phases have been observed in nanoindented silicon by Raman spectroscopy,[2,8–11] plan view,[7] and cross-sectional transmission electron microscopy (XTEM)[1–5,12–15] as well as electrical measurements.[16,17] In addition, XTEM studies, following indentation on (100) silicon, also show slip bands on {111} planes below the transformation zone. Median cracks at very low loads (20 mN) in the case of sharp indents and at higher loads after spherical indentation are also observed.

Almost all of the above investigations have been carried out on (100) Si, but, in contrast, there are only a few studies on (111)-oriented Si. For example, the high-pressure silicon phases, Si-III and Si-XII, were observed by Raman spectroscopy within indents following indentation of (111) silicon.[9–11] Furthermore, electrical resistance measurements have shown that the pressure required to induce transformation to the Si-II structure is lower in the [111] than in the [100] direction.[18] However, there have been no systematic XTEM investigations for (111) Si addressing, in detail, the subsurface microstructures developed following indentation. Therefore, in this study, the deformation microstructures beneath indentations induced in uncoated (111) Si by a spherical indenter have been characterized, and the results were compared with similar studies in (100) Si.

## II. EXPERIMENTAL PROCEDURE

The (111) Si wafer (~500-μm thick) was subjected to nanoindentation with a spherical-tipped diamond indenter of nominal tip radius 5 μm, using the UMIS-2000 (Ultra Micro-Indentation System; CSIRO, Australia). Nanoindentation was performed to loads in the range of 20 to 100 mN. A layout file was used, and the indents of interest were made in-between four high-load ones to facilitate preparation of XTEM samples. During loading and unloading, 40 increments were recorded with the unloading rates ranging from 0.3–1 mN/s. To determine the elastic modulus required for modeling, nanoindentation was also performed on the (111) Si wafer using the Hysitron Triboindenter (Minneapolis, MN) with a Berkovich indenter having a tip radius of 100 nm. The indenter was calibrated using fused silica standard, and the elastic modulus was determined following the procedure described by Oliver and Pharr.[19]

XTEM specimens were prepared from the indents using a Nova Nanolab 200 dual-beam focused-ion beam (FIB; FEI, Hillsboro, OR), and the samples were lifted out onto C-coated copper grids using an optical microscope and a glass needle attached to a piezoelectric device. The thin foils were examined normal to the <110> of the silicon substrate in a Philips CM200 TEM. Note that Saka and Nagaya[20] were the first to apply the FIB technique to TEM observation of indented Si, followed subsequently by several other researchers.[1,2,12,14,15]

[a]Address all correspondence to this author.
e-mail: ayesha@materials.unsw.edu.au
DOI: 10.1557/JMR.2009.0249

  

The stress distribution produced below the indenter tip was calculated using the ELASTICA (ASMEC; Radeberg, Germany) software package,[21] which analytically determines contact-induced elastic stresses for a Hertzian pressure distribution, based on the elastic properties of the materials. An elastic modulus of 1141 GPa and a Poisson's ratio of 0.07 was used for the diamond indenter.[22] For (111) Si, the absolute elastic modulus (146.9 GPa) determined from the measured elastic modulus (from Berkovich indentation) and Poisson's ratio of 0.26 was used.[23]

## III. RESULTS

Figure 1 shows the typical load-displacement curves obtained on indentation of (111) Si with a spherical indenter, for loads up to 100 mN. Even at the lowest load of 20 mN, the indentation behavior of Si is not considered to be purely elastic. This observation is clear from the deviation of the experimental curve from the theoretical elastic curve plotted in Fig. 1 (solid line), and this is also evident from the XTEM images to be discussed later. The theoretical elastic penetration depth for the material ($h_e$) was calculated using the equation,

$$h_e = \left(\frac{3P}{4E^*}\right)^{2/3}\left(\frac{1}{R}\right)^{1/3},$$

where $P$ is the applied load, $E^*$ is the reduced modulus, and $R$ is the radius of the indenter.

This deviation from the elastic behavior occurred at a penetration depth that ranged from 10 to 16 nm corresponding to loads that ranged from 0.45 to 0.6 mN, indicating that silicon exhibits nonelastic deformation at low loads. The load-displacement curves also show that silicon exhibits substantial elastic recovery on unloading. The maximum and residual depths of penetration and magnitude of recovery increase continuously with increasing applied load. However, the percentage of recovery initially decreases rapidly with increasing load up to 60 mN and then less rapidly with further increases in load. At the lowest load studied, the percentage of recovery was almost 83%, similar to that reported by Malkov et al.[22] for (111) Si after Berkovich indentation. However, these values are significantly larger than those reported by Berasategui and Page,[24] again following Berkovich indentation.

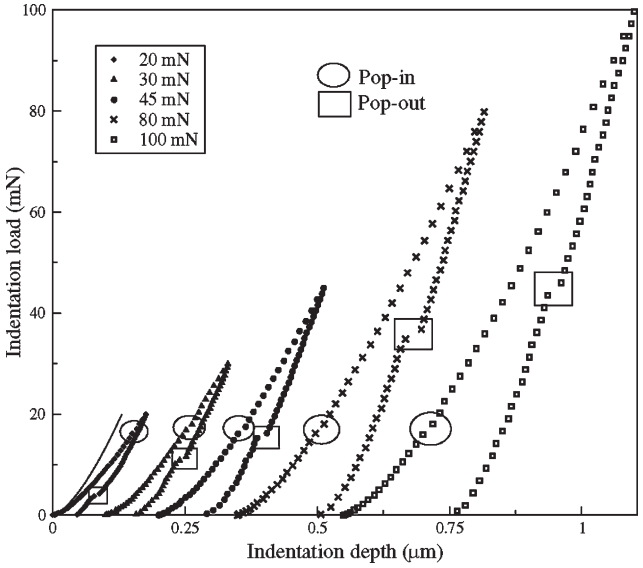


FIG. 1. Load-displacement curves for (111) Si after indentation with a spherical indenter to various maximum loads. The curves have been plotted with offsets of 0, 0.1, 0.2, 0.35, and 0.55 μm on the $x$-axis for maximum loads of 20, 30, 45, 80, and 100 mN, respectively. The theoretical elastic curve is also shown alongside.

Tables I and II show the load range at which discontinuities appear in the load-displacement curves, their mean value, and the average deviation. The discontinuity on loading appears over a small range of 15.5 to 18.5 mN over the range of loads studied. Saka et al.[12] have observed a constant load for the occurrence of pop-in event; however, the slight variation in the pop-in load observed in this study is within experimental scatter. The magnitude of the pop-in event during loading was found to be small. In contrast, the pop-out event was clearly discernible in the unloading curves. Even at very low loads of 20 mN, either an elbow or pop-out was clearly evident during unloading. At this lowest load, out of the 10 indentations performed, approximately five indents displayed an elbow, and three of them exhibited an elbow followed by pop-out, whereas the remaining two exhibited a kink pop-out. Elbow events have been reported on indentation of (100) Si with spherical[4,5] as well as Berkovich[9,14] indenters. In (111) Si also, elbow events have been observed at low loads with a Berkovich indenter.[9,10] However, during spherical indentation with a 13.5-μm radius indenter, Juliano et al.[11] have reported that the elbow events are not observed, or they are subtle and cannot be detected by normal means. These authors suggested that a smaller indenter radius might result in elbows, as has been observed in this study. The kink pop-outs at the applied load of 20 mN appear at an average load of ~7.9 mN, whereas the pop-outs following an elbow occur at a much lower load of ~4.3 mN. Juliano et al.[10,11] have reported that the average pop-out pressures for normal pop-out are higher than for pop-outs following an elbow and suggested that the elbow before the pop-out lowers the pressure at which pop-out occurs.

TABLE I. Pop-in loads for (111) Si after indentation to various loads.

| Indentation load (mN) | Pop-in load (mN) | | |
|---|---|---|---|
| | Range | Mean | Average deviation |
| 20 | 15.5–18 | 16.3 | 0.49 |
| 30 | 16–20.4 | 18.4 | 1.63 |
| 45 | 16.2–21.5 | 18.2 | 1.5 |
| 80 | 16–20 | 17.8 | 0.85 |
| 100 | 14–18 | 15.4 | 1.3 |

TABLE II. Pop-out loads and depths and percentage unloading from maximum load for (111) Si after indentation to various indentation loads (I.L.).

| | Pop-out load (mN) | | | | Pop-out depth (μm) | | |
|---|---|---|---|---|---|---|---|
| I.L. (mN) | Range | Mean | Average deviation | % Unloading from maximum load | Range | Mean | Average deviation |
| 20 | 5.5–9.5 | 7.3 | 0.76 | 63.5 | 0.09–0.13 | 0.113 | 0.01 |
| 30 | 6.5–14 | 10.5 | 2.59 | 63.3 | 0.12–0.17 | 0.142 | 0.02 |
| 45 | 16–21 | 18.97 | 1.66 | 57.77 | 0.18–0.22 | 0.212 | 0.01 |
| 80 | 28–42 | 35 | 4.5 | 56.25 | 0.31–0.36 | 0.339 | 0.02 |
| 100 | 36–52 | 43.5 | 5.4 | 56.5 | 0.35–0.42 | 0.405 | 0.02 |

As mentioned above, there were more elbows than pop-outs at 20 mN. However, for indentation loads higher than 45 mN, only one elbow event and one elbow followed by a pop-out event were observed, the remaining being distinct pop-outs, whereas no elbow events were present for loads above 80 mN, with all the curves showing a distinct pop-out. Therefore, the probability of the occurrence of either elbows and elbows followed by pop-outs decreased, and that of distinct pop-outs increased with increasing applied load, similar to the observations of Juliano et al.[10,11] It is clear from Table II that the mean pop-out load and the indent penetration at the pop-out increase with an increase in indentation load, as reported by several earlier studies.[3,10–12] Juliano et al.[11] have suggested that the larger the applied load, the larger the volume of material under transformation pressure beneath the indenter, the more thermodynamically unstable it is and thus it transforms at a higher load. Table II also shows the penetration depth of indenter and the percentage of unloading from maximum applied load at which pop-out events appear in the load-displacement curve. It is evident from the table that, for all the loads studied, the pop-out event appears on unloading to beyond 50% of the maximum load, similar to the observations of Ruffell et al.[15] for (100) Si.

Figures 2(a) and 2(b) show the subsurface microstructures developed in (111) Si after indentation to a load of 20 mN. Indentation at this low load was performed between two closely spaced neighboring indents of 100 mN, applied for assistance in locating the low load indents for TEM sample preparation. The XTEM sample prepared at this load also includes the two high load indents, which are clearly visible on either side of the 20 mN indent [Fig. 2(a)]. Beneath the protective Pt layer that was deposited in the FIB, a thin (~40–45-nm thick) and continuous layer of amorphous silicon, labeled K, is visible all along the length of the XTEM specimen. The amorphous layer was present in all the XTEM images and has also been observed by other authors in XTEM samples of (100) Si and is reported to be a result of gallium ion implantation during imaging in the FIB before Pt deposition.[1,2,12,25]

Even at this low load of 20 mN [Fig. 2(b)], the region labeled X clearly exhibits contrast different from that of bulk silicon, labeled Y, indicating that the hydrostatic stresses developed beneath the indenter tip are sufficient to cause phase transformation in the silicon. It is known that hydrostatic stresses cause the transformation of Si-I to Si-II.[26–28] The size of this transformation zone developed beneath the indenter tip is approximately ~1.25 μm wide and ~160 nm deep. Unlike the hemispherical transformation zone observed at low loads on spherical indentation of (100) Si,[1–3] the transformation zone seen in Fig. 2(b) appears to have a more conical shape. Zarudi and Zhang[3] have reported that the transformation zone tends to be hemispherical at low loads, but it approaches a more conical shape at higher loads (above 90 mN). However, in this study, the transformation zone is conical

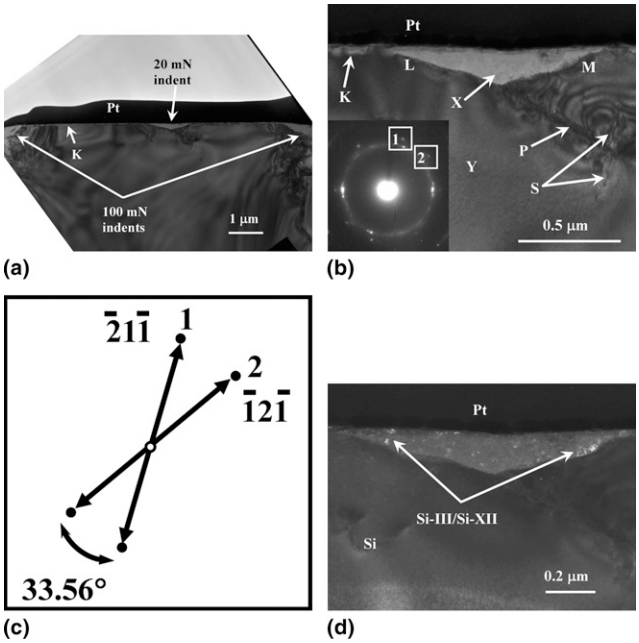


FIG. 2. (a) Bright-field (BF) XTEM image of (111) Si after indentation to a load of 20 mN showing two 100 mN indents, with the 20 mN indent in between, and the continuous amorphous layer (K). (b) Magnified image of the 20 mN indent showing phase transformation zone (X), slip band (P), and dislocations (S); inset shows the SADP from the transformation zone. (c) Key diagram to SADP. (d) Dark-field (DF) image, taken using reflection 1, showing contrast from the high-pressure phases.

in shape even at this low load. It was found that the edges, marked L and M, of the transformation zone were oriented almost parallel to the {211} and {331} planes, respectively, of the diamond cubic Si-I phase.

In addition to strong reflections from the Si-I phase (due to the diameter of the selected area diffraction aperture being larger than the size of the zone), the selected area diffraction pattern (SADP) taken from the transformation zone [inset in Fig. 2(b)] exhibits diffuse rings characteristic of a-Si, as well as reflections from the high-pressure crystalline phases. The key diagram to the SADP [Fig. 2(c)] shows that two of these reflections, labeled 1 and 2, have an interplanar spacing of 0.271 nm and are indexed to be consistent with {211} planes of the body-centered cubic Si-III.[28,29] Furthermore, the interplanar angle of 33.6° between these reflections suggests that they belong to the [$\bar{1}$13] zone axis of this phase. The dark-field image [Fig. 2(d)], taken using reflection 1, shows fine, dispersed grains of the high-pressure crystalline phases in the transformation zone within an amorphous silicon phase.

Similar to observations following indentation on (100) Si to the same load,[1–5,12] plastic deformation is observed beneath the transformation zone. The slip band, labeled P, which extends to a depth of ~450 nm, as well as dislocations, labeled S, are evident in Fig. 2(b). The slip band P is oriented at an angle of 29.5° to the (111) surface, indicating that it is aligned parallel to the {311} planes of the single-crystal silicon, unlike (100) Si, where the slip bands are usually aligned parallel to the {111} planes of Si. The dislocations, labeled S, nevertheless are oriented along {111} planes. In other words, they are inclined at an angle of 70° to the surface of the sample. In addition to the penetration depths of the defects being less that in (100) Si,[1–5,12] the dislocation density is also significantly lower in (111) Si. Moreover, the slip bands appear only adjacent to the transformation zone and not directly beneath the indenter tip, unlike that observed in (100) Si.

The subsurface microstructure developed further on indentation to a load of 30 mN is shown in Fig. 3(a). With an increase in the applied load, the size of the transformation zone, labeled X, increased, as did the concentration of the crystalline phases within it. The phase transformation zone measures ~275 nm in depth and ~1.55 μm wide. Again, similar to observations at the lower load, the edges L and M of the transformation zone were oriented almost parallel to the {211} and {331} planes of Si-I phase, respectively. Furthermore, the boundary L appears to become parallel to a {311} plane in the region labeled N.

The inset in Fig. 3(a) shows the diffraction pattern taken from the transformation zone, which displays diffuse rings indicative of a-Si, as well as several intense reflections from the high-pressure phases. Therefore, the

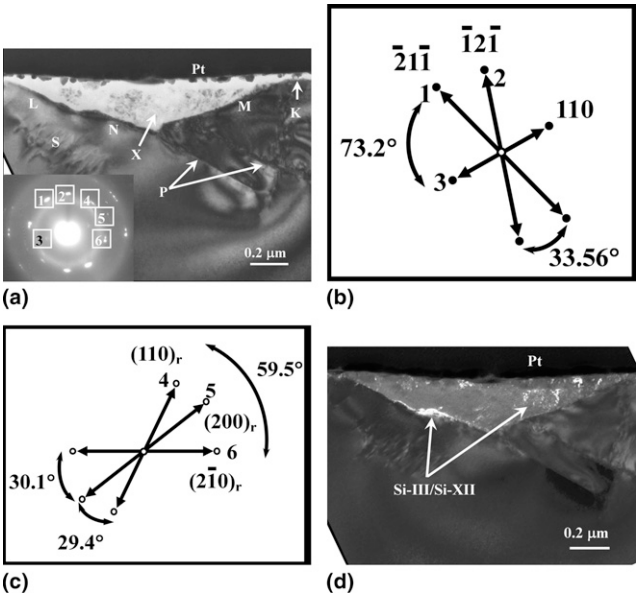


FIG. 3. (a) BF XTEM image of (111) Si after indentation to a load of 30 mN, showing phase transformation zone (X), slip bands (P), and dislocations (S); inset shows the SADP from the transformation zone. (b) Key diagram to SAPD for Si-III phase. (c) Key diagram to SAPD for Si-XII phase. (d) DF image, taken using the reflection 3, showing contrast from the high-pressure phases.

analysis performed for this diffraction pattern has been depicted in two key diagrams: one involving reflections 1, 2, and 3 (shown as closed circles) for the cubic Si-III phase [Fig. 3(b)], and the other involving reflections 4, 5, and 6 (shown as open circles) for the rhombohedral Si-XII phase [Fig. 3(c)]. In Fig. 3(b), it is evident that reflections 1 and 2, with interplanar spacings of 0.271 nm, arise from the {211} planes and reflection 3 with a spacing of 0.469 nm, from the {110} planes of Si-III phase, having a lattice parameter of 0.664 nm. The interplanar angle of 33.56° between the {211} planes and that of 73.2° between {110} and {$\bar{2}$11} planes suggest that these reflections belong to the [$\bar{1}$13] zone axis of the body-centered cubic Si-III phase. Figure 3(c) shows that reflections 4, 5, and 6 with interplanar spacings of 0.257, 0.225, and 0.263 nm arise from {110}, {200}, and {2$\bar{1}$0} planes of the rhombohedral Si-XII phase, respectively, having a lattice parameter a = 0.561 nm and $\gamma$ = 110.07°. The values of lattice parameter are consistent with the values reported by George[29] for the Si-XII phase. Furthermore, the interplanar angle of 29.4° between the {110} and {200} planes, 30.1° between the {200} and {2$\bar{1}$0} planes, and 59.5° between the {110} and {2$\bar{1}$0} planes is consistent with the [001] zone axis of the rhombohedral Si-XII phase.

The dark-field image, shown in Fig. 3(d), obtained by selecting reflection 3, shows a larger volume of the high-pressure crystalline phases than that observed at the lower load. Below the transformation zone, the number and length of the slip bands, labeled P, increase to a maximum

penetration depth of ~650 nm [Fig. 3(a)]. Again, the slip bands are aligned parallel to the {311} planes of Si-I. The residual contrast from a few dislocations, labeled S, is also seen on the side opposite of the slip band.

With a further increase in the indentation load to 45 mN, the transformation zone (labeled X) increased to a depth of ~326 mN and a width of ~1.85 μm (Fig. 4). The orientation of the boundary M is along {331}, similar to that observed at the lower loads. However, the edge around boundary L appears to be parallel to {311}, whereas edge N is close to the {211} planes of Si-I.

SAD analysis of the transformed zone again revealed the presence of Si-III and Si-XII. The increase in the applied load also increased the number and length of the slip bands (P and Q) below the transformation zone. These slip bands P and Q are again aligned along the {311} planes. However, unlike observations on (100) Si, even at this load there are no slip bands or dislocations in the central region below the transformation zone, and the extent of deformation of diamond cubic silicon below the transformation zone is significantly less as compared with (100) Si.

Following indentation to a maximum load of 80 mN, bending at the surface due to the indentation is clearly visible in Fig. 5. The transformation zone (labeled X) developed beneath the indenter tip measures 540 nm deep and 2.59 μm wide. Again, edges L and M of the transformation zone appear to be oriented close to {311} planes. Analysis of SAD patterns from this region is consistent with the presence of Si-III. Below the transformation zone, the penetration depth of slip bands, labeled P, has increased to ~1.45 μm; however, their density has not increased. Residual contrast from dislocations, labeled S, is also observed.

With a further increase in load to 100 mN [Fig. 6(a)], there is significant bending at the surface. The depth of the residual indent imprint was measured as ~185 nm.

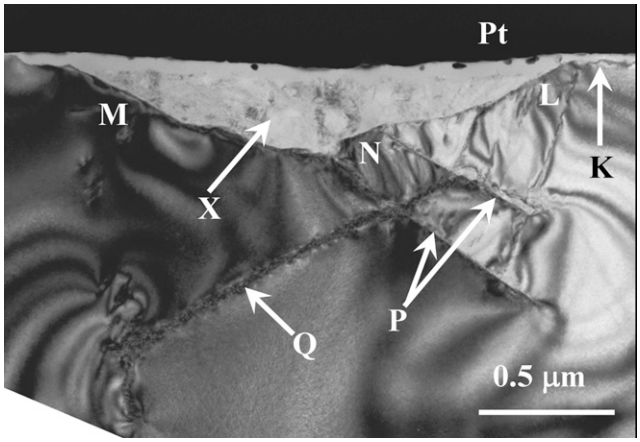


FIG. 4. BF XTEM image of (111) Si after indentation to a load of 45 mN, showing phase transformation zone (X) and slip bands (P, Q).

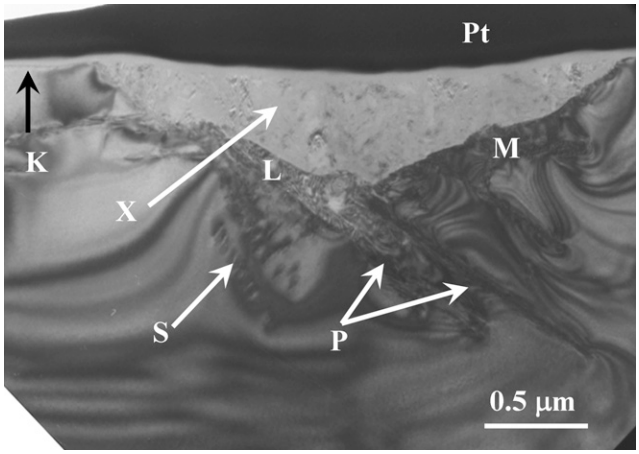


FIG. 5. BF XTEM image of (111) Si after indentation to a load of 80 mN, showing phase transformation zone (X), slip bands (P), and dislocations (S).

The transformation zone (labeled X) also increased to ~564 nm deep and ~2.9 μm wide. Again, the SADP from the transformation zone clearly showed strong reflections from the silicon high-pressure phases. In Fig. 6(a), as well as in the magnified image [Fig. 6(b)], a small region, labeled Z, within the transformation zone exhibits a contrast distinct from the surrounding high-pressure phases. A SADP [inset in Fig. 6(b)], taken from this region, indicates that it is untransformed diamond cubic silicon. A microcrack, labeled 2, is also visible in the transformation zone. Below the transformation zone [Fig. 6(a)], the penetration depth of the slip bands has reduced slightly to 1.44 μm. However, the overall extent of deformation has increased significantly compared with that observed at lower loads. In addition to slip bands, labeled P, aligned on {311} planes of silicon, a few slip dislocations, labeled S, oriented along the {111} planes are also evident. Furthermore, dislocations, labeled R, parallel to the surface, i.e., along the {111} planes, are also visible and are shown at a higher magnification in Fig. 6(c).

Similar to the observations of Zarudi and Zhang[3] for indentation of (100) Si to a load of 100 mN, a median crack is visible in the diamond cubic silicon below the transformation zone [Fig. 6(a)]. The median crack is reported to nucleate at the intersection of the slip bands and extend down into the bulk of the crystal. In the region where slip bands intersect, dislocations pile up and presumably act as barriers to further dislocation glide. This dislocation pile-up at the extremity of slip bands is likely to cause stress concentration resulting in the nucleation of a microcrack.

## IV. DISCUSSION

It is evident from Table II that the pop-out load increases almost linearly with the maximum applied load.

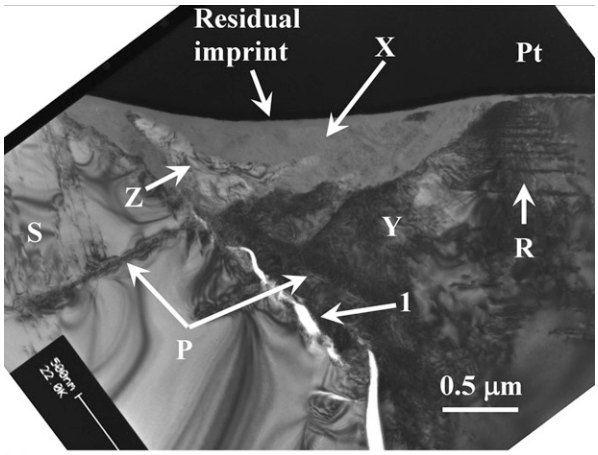


(a)

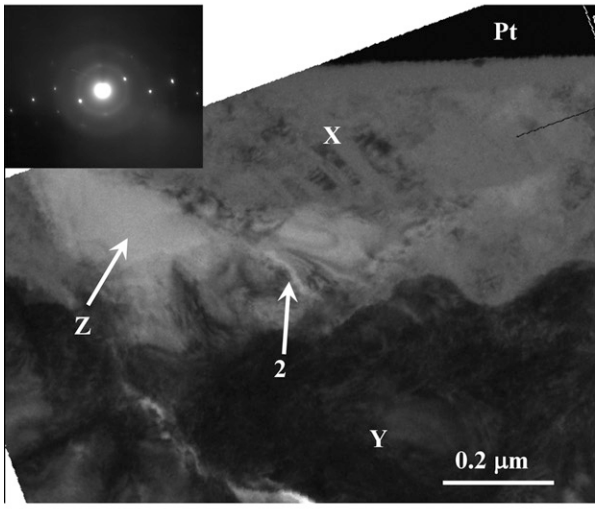


(b)

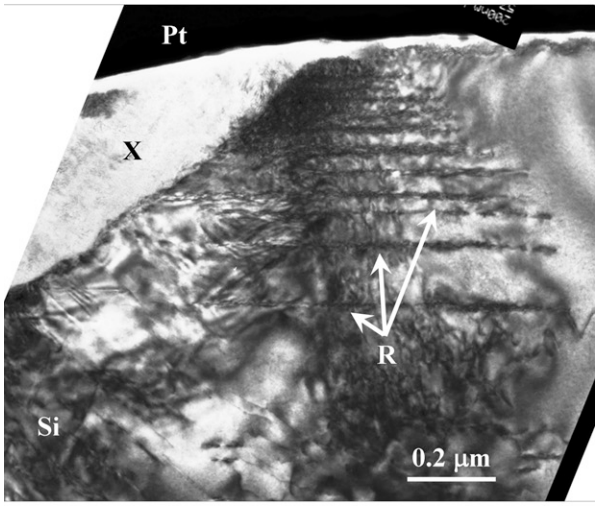


(c)

FIG. 6. (a) BF XTEM image of (111) Si after indentation to a load of 100 mN showing phase transformation zone (X), slip bands (P), and dislocations (S, R). (b) Magnified image of transformation zone showing the presence of untransformed Si in region Z. Inset shows SADP from this region. (c) Magnified image showing contrast from dislocations, labeled R.

This variation, plotted in Fig. 7 (solid line), is similar to the plot of the pop-out pressure against applied load reported by Juliano et al.[10] for Berkovich indentation of (111) Si. A similar variation for the indent penetration at pop-out with applied load is shown in Fig. 7 as a dotted line. However, Zarudi and Zhang[3] have observed two different slopes for pop-outs during spherical indentation of (100) Si and related them to changes in the different structures (amorphous and the crystalline phases) observed in the transformation zone at low and high loads, respectively. However, in this study, even at a low load, significant amounts of crystalline phases are observed in the transformation, resulting in an almost linear variation.

The experimentally measured depth and width of the transformation zone as well as the extent of defect penetration observed at different maximum applied loads are summarized in Table III and also plotted in Fig. 8. The depth and width of the transformation zone increase almost linearly with increasing load. This result is inconsistent with the observations of Zarudi and Zhang[3] for spherical indentation on (100) Si. These authors have reported that the depth of transformation zone increases proportionally with load, but the width of the zone does not. Furthermore, it is clear from Fig. 8 that the depth of defect penetration increases rapidly up to a load of 60 mN, reaches a plateau between 60 and 80 mN, and then decreases slightly with an additional increase in load to

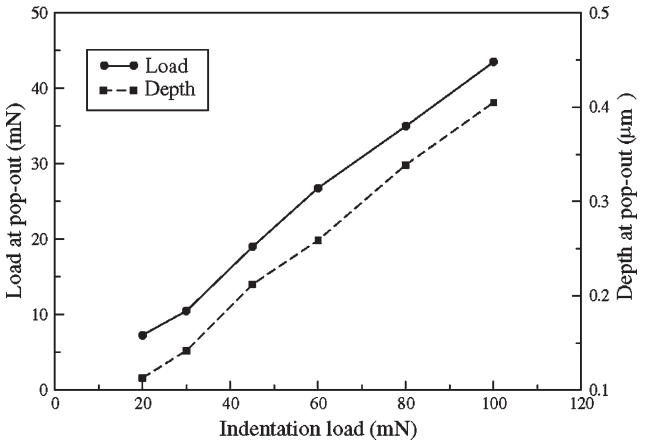


FIG. 7. Variation of load at pop-out and indent penetration at pop-out with indentation load.

TABLE III. Transformation zone size and defect penetration measured from XTEM images.

| Load (mN) | Transformation zone size (μm) | | Depth of defect penetration (μm) |
|---|---|---|---|
| | Depth | Width | |
| 20 | 0.16 | 1.25 | 0.45 |
| 30 | 0.27 | 1.55 | 0.65 |
| 45 | 0.32 | 1.85 | 1.13 |
| 80 | 0.54 | 2.59 | 1.45 |
| 100 | 0.56 | 2.89 | 1.45 |

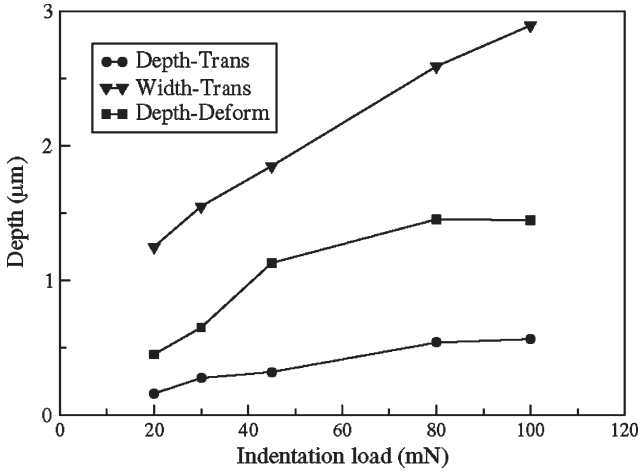


FIG. 8. Variation of the depth and width of transformation zone and the defect penetration depth with indentation load.

100 mN. Zarudi and Zhang[3] have also observed a similar variation in defect penetration and related it to the initiation of microcracks at the intersection of defects. They suggested that the relaxation occurring in the material due to the onset of microcracks could prevent further penetration of defects. This observation is confirmed by the presence of a median crack at the intersection of defects after indentation to 100 mN.

If the magnitudes of these experimentally measured parameters are compared with those reported by Zarudi and Zhang[3] on (100) Si, it is evident that the depth of defect penetration observed in this study is marginally lower than the values on (100) Si, for all loads. The depth of the transformation zone, on the other hand, is slightly higher than the values on (100) Si at lower loads and lower at higher loads. In contrast, the width of the transformation zone, observed in this study, is significantly larger at lower loads and becomes comparable at higher loads. Comparison of the depth and width of transformation zone with those reported by Bradby et al.[1,2] on (100) Si again reveal that the depth of the zones observed in this study are significantly larger and the width of the zones are comparable. These data suggest that the transformation zone size observed in this study on (111) Si is larger than those reported for (100) Si, especially at lower loads. It has been reported that the pressure required to induce transformation to the Si-II structure is lower in the [111] than in the [100] direction.[17] This effect apparently results in a larger volume of transformation especially at lower loads, as observed in this study. For the same reason, it is possible that the extent of overall deformation observed in (111) Si is significantly lower, because most of the applied load is taken up for transformation of the diamond cubic silicon.

A major difference observed between the subsurface microstructures developed on indentation in (100) Si and (111) Si is with respect to the nature of defects developed beneath the indenter tip. Instead of the slip occurring on the {111} planes of silicon, the slip bands that develop below the transformation zone are aligned parallel to the {311} planes, indicating that during indentation of (111) Si, slip occurs at a lower shear stress along the {311} planes rather that on {111} planes. Moreover, as mentioned earlier, the number of slip bands, as well as the penetration of defects, is significantly lower than those observed on indentation of (100) Si, except at a load of 100 mN. Furthermore, the distribution of defects also appears to be different from that observed in (100) Si. The defects consistently appear on either side of the central region of the transformation zone but not directly beneath the central region, unlike in (100) Si. These observations seem to be consistent with the findings of Yoshino et al.[30] who have simulated dislocation generation and propagation during indentation on (111) Si. Using finite element simulation, these authors have shown that the distribution of dislocations is not symmetric, due to the anisotropy of lattice orientation. Furthermore, their model showed an absence of dislocations directly beneath the center of the indent, consistent with the observations in this study.

## V. ELASTICA SIMULATIONS

The critical von Mises stress ($\sigma_M$) for plastic deformation in Si has been reported as $11.2 \pm 0.08$ GPa.[31,32] Therefore, $\sigma_M$ in the material should exceed values of this order for yielding to occur. On the other hand, the hydrostatic stresses ($\sigma_H$) associated with the Hertzian stress fields beneath the indenter are reported to be responsible for phase transformation in the silicon substrate.[26–28] Although the accepted value for the transformation of Si-I to Si-II under pure hydrostatic stress is of the order of 11.3–12.5 GPa,[27,28] the presence of shear stresses during indentation has been reported to lower the transformation pressure to 8 GPa.[18,33] Therefore, it can be assumed that values of this order are required for phase transformation.

The isobaric plots of $\sigma_M$ and $\sigma_H$ generated in the XZ plane after indentation with a spherical indenter to a load of 20 mN are shown in Figs. 9(a) and 9(b), respectively. The maximum $\sigma_M$ [Fig. 9(a)] value of 11.22 GPa (indicated by '+') is located at a depth of ~0.34 μm beneath the surface. On the other hand, the maximum $\sigma_H$ [Fig. 9(b)] of 14.76 GPa is situated at the surface of the sample. The simulation results suggest that (111) Si loaded to 20 mN is expected to exhibit phase transformation as well as plastic deformation beneath the indenter tip. XTEM below the indenter after indentation to a load of 20 mN (Fig. 2) clearly indicates a phase transformation zone beneath the indenter tip as well as plastic deformation below the transformation zone with the slip bands extending to depths of 450 nm beneath the surface.

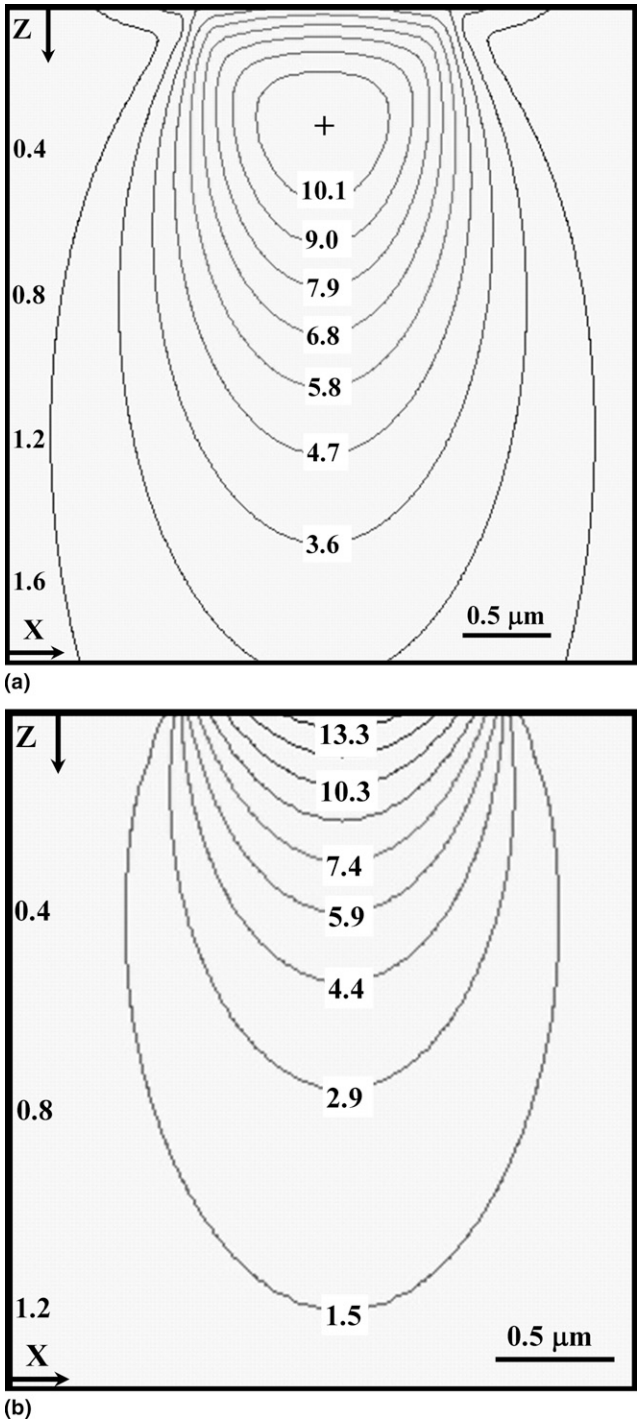


FIG. 9. Simulated stress (GPa) contours generated in the XZ plane after indentation of (111) Si to 20 mN (a) $\sigma_M$ (b) $\sigma_H$.

Increases in the indentation load to higher values increase the magnitude of $\sigma_M$ and $\sigma_H$ developed in the material. Consequently, this activity results in a larger transformation zone, as well as a higher degree of plastic deformation in Si as is evident in the XTEM images after indentation to higher loads.

## VI. CONCLUSIONS

Spherical indentation on (111) Si results in pop-in at a constant average load of approximately 16 mN, whereas the pop-out load increases with an increase in load. A phase transformation zone comprising high-pressure Si-III/Si-XII phases is observed even at very low loads of 20 mN, indicating that the pop-in in the loading curve is a consequence of phase transformation. The volume of the transformation zone, as well as the extent of the crystalline phases, increases with increasing load. Unlike indentation on (100) Si, slip bands are mainly activated on {311} planes of Si-I. Furthermore, the density of defects is significantly lower and their distribution is asymmetric. On indentation to a load of 100 mN, a median crack developed below the transformation zone.

## ACKNOWLEDGMENTS

We thank Drs. Avi Bendavid and Phil Martin (Department of Materials Science and Engineering, CSIRO, Lindfield, Australia) for providing the (111) Si wafer used in this investigation.

## REFERENCES

1. J.E. Bradby, J.S. Williams, J. Wong-Leung, M.V. Swain, and P. Munroe: Transmission electron microscopy observation of deformation microstructure under spherical indentation in silicon. *Appl. Phys. Lett.* **77,** 3749 (2000).
2. J.E. Bradby, J.S. Williams, J. Wong-Leung, M.V. Swain, and P. Munroe: Mechanical deformation in silicon by micro-indentation. *J. Mater. Res.* **16,** 1500 (2001).
3. I. Zarudi and L.C. Zhang: Structure changes in monocrystalline silicon subjected to indentation-experimental findings. *Tribol. Int.* **32,** 701 (1999).
4. I. Zarudi, L.C. Zhang, and M.V. Swain: Microstructure evolution in monocrystalline silicon in cyclic microindentations. *J. Mater. Res.* **18,** 758 (2003).
5. I. Zarudi, J. Zou, and L.C. Zhang: Microstructures of phases in indented silicon: A high resolution characterization. *Appl. Phys. Lett.* **82,** 874 (2003).
6. V. Domnich and Y. Gogotsi: Phase transformations in silicon under contact loading. *Rev. Adv. Mater. Sci.* **3,** 1 (2002).
7. D. Ge, V. Domnich, and Y. Gogotsi: High-resolution transmission-electron-microscopy study of metastable silicon phases produced by nanoindentation. *J. Appl. Phys.* **93,** 2418 (2003).
8. A. Kailer, Y.G. Gogotsi, and K.G. Nickel: Phase transformations of silicon caused by contact loading. *J. Appl. Phys.* **81,** 3057 (1997).
9. V. Domnich, Y. Gogotsi, and S. Dub: Effect of phase transformations on the shape of the unloading curve in the nanoindentation of silicon. *Appl. Phys. Lett.* **76,** 2214 (2000).
10. T. Juliano, Y. Gogotsi, and V. Domnich: Effect of indentation unloading conditions on phase transformation induced events in silicon. *J. Mater. Res.* **18,** 1192 (2003).
11. T. Juliano, V. Domnich, and Y. Gogotsi: Examining pressure-induced phase transformations in silicon by spherical indentation and Raman spectroscopy. *J. Mater. Res.* **19,** 3099 (2004).
12. H. Saka, A. Shimatani, M. Suganuma, and Suprijadi: Transmission electron microscopy of amorphization and phase transformation beneath indents in Si. *Philos. Mag. A* **82,** 1971 (2002).

13. I. Zarudi, L.C. Zhang, W.C.D. Cheong, and T.X. Yu: The difference of phase distributions in silicon after indentation with Berkovich and spherical indenters. *Acta Mater.* **53,** 4795 (2005).
14. J. Yan, H. Takahashi, X. Gai, H. Harada, J. Tamaki, and T. Kuriyagawa: Load effects on the phase transformation of single-crystal silicon during nanoindentation tests. *Mater. Sci. Eng., A* **423,** 19 (2006).
15. S. Ruffell, J.E. Bradby, J.S. Williams, and P. Munroe: Formation and growth of nanoindentation-induced high pressure phases in crystalline and amorphous silicon. *J. Appl. Phys.* **102,** 063521 (2007).
16. J.E. Bradby, J.S. Williams, and M.V. Swain: In situ electrical characterization of phase transformations in Si during indentation. *Phys. Rev. B: Condens. Matter* **67,** 085205 (2003).
17. S. Ruffell, J.E. Bradby, N. Fujisawa, and J.S. Williams: Identification of nanoindentation-induced phase changes in silicon by in situ electrical characterization. *J. Appl. Phys.* **101,** 083531 (2007).
18. M.C. Gupta and A.L. Ruoff: Static compression of silicon in the [100] and in the [111] directions. *J. Appl. Phys.* **51,** 1072 (1980).
19. W.C. Oliver and G.M. Pharr: An improved technique for determining hardness and elastic modulus using load and displacement sensing indentation experiments. *J. Mater. Res.* **7,** 1564 (1992).
20. H. Saka and G. Nagaya: Plan-view transmission electron microscopy observation of a crack tip in silicon. *Philos. Mag. Lett.* **72,** 251 (1995).
21. T. Chudoba and N. Schwarzer: ELASTICA software package version 3, http://www.asmec.de/.
22. T. Malkow, I. Arce-Garcia, A. Kolitsch, D. Schneider, S.J. Bull, and T.F. Page: Mechanical properties and characterisation of very thin CN*x* films synthesised by IBAD. *Diamond Relat. Mater.* **10,** 2199 (2001).
23. http://www.ioffe.rssi.ru/SVA/NSM/Semicond/Si/mechanic.htm.
24. E.G. Berasategui and T.F. Page: The contact response of thin SiC-coated silicon systems-characterization by nanoindentation. *Surf. Coat. Technol.* **163–164,** 491 (2003).
25. B. Haberl, J.E. Bradby, S. Ruffell, J.S. Williams, and P. Munroe: Phase transformations induced by spherical indentation in ion-implanted amorphous silicon. *J. Appl. Phys.* **100,** 013520 (2006).
26. G.M. Pharr, W.C. Oliver, and D.S. Harding: New evidence for a pressure-induced phase transformation during the indentation of silicon. *J. Mater. Res.* **6,** 1129 (1991).
27. E.R. Weppelmann, J.S. Field, and M.V. Swain: Observation, analysis, and simulation of the hysteresis of silicon using ultra-micro-indentation with spherical indenters. *J. Mater. Res.* **8,** 830 (1993).
28. J.Z. Hu, L.D. Merkle, C.S. Menoni, and I.L. Spain: Crystal data for high-pressure phases of silicon. *Phys. Rev. B: Condens. Matter* **34,** 4679 (1986).
29. A. George: *Properties of Crystalline Silicon*, edited by R. Hull (Inspec, London, 1999), p. 104.
30. M. Yoshino, T. Aoki, N. Chandrasekaran, T. Shirakashi, and R. Komanduri: Finite element simulation of plane strain plastic-elastic indentation on single-crystal silicon. *Int. J. Mech. Sci.* **43,** 313 (2001).
31. T. Chudoba, N. Schwarzer, and F. Richter: Steps towards a mechanical modeling of layered systems. *Surf. Coat. Technol.* **154,** 140 (2002).
32. T. Chudoba, M. Griepentrog, A. Duck, D. Schneider, and F. Richter: Young's modulus measurements on ultra-thin coatings. *J. Mater. Res.* **19,** 301 (2004).
33. J.J. Gilman: Shear-induced metallization. *Philos. Mag. B* **67,** 207 (1993).